Early Photon Optical Tomography.

Vasilis Ntziachristos, Antoine Soubret, Gordon Turner.

***Abstract*—Fluorescence tomography is an emerging tool for functional and molecular imaging of tissues. Inversion is however complicated by the high scattering that photons experience when propagating through tissue that reduces resolution. While continuous wave systems offer implementation simplicity, time-resolved systems offer the ability to improve resolution and reduce the ill-posed nature of the inverse problem by using early arriving photons. We present an overview of our current progress in complete-angle illumination early photon tomography and present the associated data processing steps employed for early photon inversions.**

***Index Terms*— Optical tomography, Fluorescence, molecular imaging.**

I. Introduction

Fluorescence molecular tomography (FMT) has recently emerged as an important alternative for molecular imaging of whole tissues [1, 2]. The technology is far from being fully explored however; light and associated fluorescence chemistries offer several unique contrast mechanisms [3] and interactions with tissues that can yield significant mechanisms for visualizing an increasing number of complex biological processes in-vivo[4-6]. It is further important to develop robust imaging systems and inversion techniques that can yield accurate visualization of the fluorescence bio-distributions of different fluorescent probes with molecular specificity. Similarly, signal processing and noise handling become important determinants of imaging performance, especially as the technology continues to emerge and approaches physical limits[7, 8].

Imaging with early photons offers an elegant way to improve resolution and tomographic performance [3,9]. Photons collected shortly after an ultra-fast pulse is launched into a diffusive medium experience significantly fewer scattering events and travel preferentially around a straight line connecting the source to the detector. Therefore they can be used to effectively reduce the high blurring that occurs when the bulk of injected photons are used, or equivalently when light of constant intensity is employed for imaging.

The resolution achieved in systems employing constant intensity light illumination has been recently measured for small animal imaging related dimensions and was found to be in the sub-millimeter range for the near-infrared spectral window [10]. This resolution figure is significant considering the high photon diffusion in tissues and has been achieved due to the high spatial sampling of photon profiles and appropriate inversion schemes that can partially account for the highly diffusive nature of photon propagation in tissues. While corresponding studies have not been performed yet with early photon systems of similar refinement, it is expected that the resolution achieved in such early-photon systems would be significantly better, possibly reaching no more than a few hundred microns for small animal dimensions. It is important to further note however that there are significant computation challenges in optical tomography such as inversion of increasingly large data sets and additional complexities associated with unique features of photon technology such as appropriate consideration of tissue-air boundary effects. These issues become especially crucial for high-performance optical tomography systems since, similarly to X-ray computer tomography (CT) it is important to illuminate from a large number of angles. This is especially important when early photon are employed since tomographic principles approach those used in X-ray CT. Appropriate data collection and processing schemes are also required for improving the tomographic performance. In the following we give a brief account of major data features employed in early photon tomography, for the purposes of the 2005 ICASSP conference.

II. Experimental Setup and Methods

A. Experimental Systems

Figure 1 shows a schematic of the optical imaging setup used for early photon investigations in this work. The system uses ultrafast pulses of light (~100 fs) from a mode-locked Ti:Sapphire laser oscillator that are coupled into the sample via a free-space scanning system (Nutfield Technology). The imaging chamber has input and output anti-reflective glass windows of variable separation distance to accommodate samples up to 2.5 cm in thickness. Samples are suspended in the imaging chamber from the top by a rotation stepper motor (Newport PR50pp). The scanning area can be dynamically adjusted to accommodate fields of view up to 6 x 6 cm, with user-specifiable source patterns. Furthermore, high power delivery and a wide tuning range (visible to NIR) can be achieved due to the use of achromatic optical components and a wavelength adjustable input collimation system. The

The authors are with the Laboratory for Bio-optics and Molecular Imaging at the Center for Molecular Imaging Research at the Massachusetts general Hospital and Harvard Medical School, CNY 149 13th street r.5209, Charlestown MA 02129. The e-mail of the first author is vasilis@helix.mgh.harvard.edu.

chamber is made water-tight to allow dual operation with or without matching fluids.

Images are collected with a time-gated intensified CCD camera (LaVision Picostar HR12, LaVision GmbH, Goettingen, Germany). The intensifier is triggered by the output of the laser, and an electronic delay generator is used to select the opening time of the intensifier. The intensifier remains open for 200 ps, and the delay line can select opening times in increments of 25 ps. For these experiments the temporal offset of the delay line is set to catch the earliest measurable photons transmitted by the diffusive sample.

One image is collected for each of 45 source positions, spaced every 0.4 mm in a line perpendicular to the axis of rotation. A 46th source is positioned far outside of the area of the rods to serve as an internal intensity reference for each projection angle. Angular projections were incremented in 72 five degree steps for full 360 degree coverage.

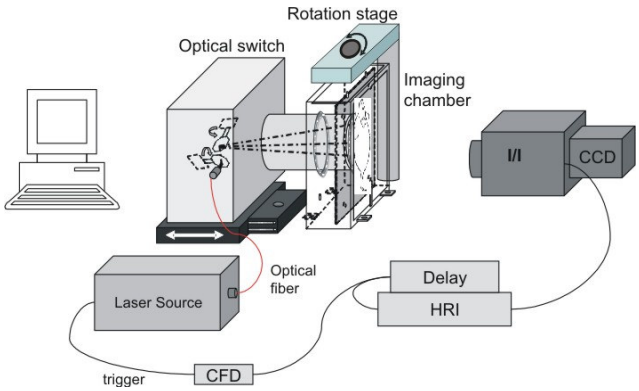

Fig. 1. Schematic view of the imaging system

The scanner developed is a generalized design that allows great flexibility in obtaining different data sets, including time-resolved measurements of the full spatial beam profile emitted from a diffusing medium, complete time-resolved curves, as well as pseudo-continuous wave (integrated over time) data. Therefore it is optimized for high versatility and the ability to detect "off axis" components of the transmitted beam profile. Similar systems have been developed for CW measurements and details can be found in Ref. [10].

B. Phantoms

For demonstration of key processing steps in employing early photon measurements we report on results obtained with a tissue-mimicking phantom, previously developed [11], with optical properties that are matched to those of mice by addition of titanium dioxide particles (for scattering) and pigment (for absorption) to a clear acrylic resin. The resin is machined into rods with cross-sectional profiles of a triangle and a square. These rods are suspended in the chamber and surrounded by a water-based tissue-mimicking optical matching fluid composed of intralipid (for scattering) and ink (for absorption) in concentrations such that the optical properties are (μ_a=0.1 cm^{-1} μ_s'= 7 cm^{-1}). The phantom is then rotated around its center axis.

III. DATA COLLECTED & RESULTS

Data pre-processing can lead to optimal data sets that can increase the accuracy of the corresponding reconstructed image. Herein we discuss measurements that are appropriate for imaging attenuation through tissues, although imaging of fluorescence follows similar rules. Generally, there are three types of measurements obtained for each source detector pair. The first measurement is taken through a homogeneous diffusive medium, in this case the optical matching fluid in the absence of the absorbing rod heterogeneities. There is no need for rotation in this case because the medium is homogeneous, so only 46 images are collected. The second measurement is taken with the image sample in place. For each source position and each rotation angle an image is acquired. For 45 source scanning positions and 5^0 step rotations this results in the collection of 3240 images in total. This number is reported for two-dimensional reconstructions. For three dimensional reconstructions of the same volume the data set can quickly reach sizes of 150,000 images (data-points) or more. The dataset utilized in these reconstructions is a sub-set of the collection potential of the system as only one time-gate was used, and from those images only a few pixels closest to the center of the source position ("on-axis projections") were extracted from the data set and used in the reconstruction.

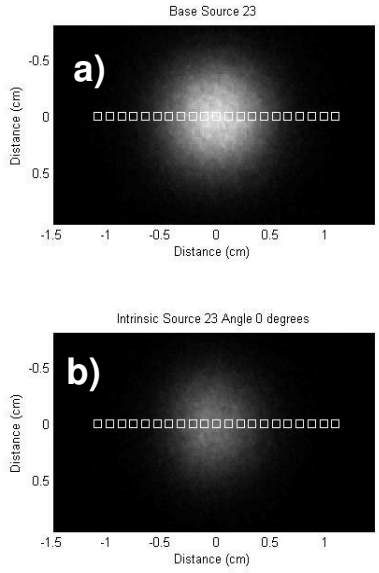

Fig. 2. Images collected for a single source position measurement through (a) a homogenous medium and (b) through a phantom. Pixels in each image can be grouped together to yield a number of virtual detectors. White boxes here show an example of a one dimensional array of detectors that can be assumed on the images collected.

Figure 2 illustrates the first part of the data post-processing that takes place prior to image reconstruction. Images from a

single source position are shown for the case of homogeneous base file (Figure 2a) and for the case of the intrinsic measurement with the rods in place at a rotation angle of 0 degrees (Figure 2b). Overlaid on top of each of these images is a representation of the virtual detectors (square boxes) that are formed by averaging a specified number of pixels from the original image (in this case a square of area 0.1 cm^2). This serves as a noise filtering step and also reduces the dimensionality of the resultant reconstructions to make them more computationally tractable. Images are generally pre-processed using median filtering to reduce shot noise.

The values extracted from these detectors are shown in Figures 3 (a) and (b) respectively. Typically constraints can be placed on these results to select only those detector readings above a specified threshold value. An alternative would be to apply adaptive thresholds or weights in each of these methods according to its specific noise characteristics (either explicitly or through employment of appropriate inversion routines[7, 8]) although this step was not followed herein. Instead we selected only those detectors closest to the center of the source position (the on-axis detectors) for each image. This scalar intensity is then stitched together with those values from each of the other 45 sources in a given angular projection to create a "line scan" across the sample.

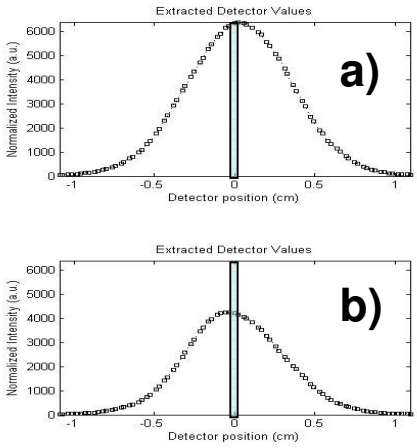

Fig. 3. Photon profiles collected with the virtual detectors indicated as white boxes on the images of Fig.2.

Figure 4(a) shows the phantom employed and Fig.4(b) and (c) illustrate two corresponding line scans collected at projection angles of 0 and 90 degrees respectively. The inset in Fig.4 (b) and (c) depict the relative orientation of the phantom. The y-axis on these figure is the normalized Born field used in the inversion method, which is $U_{nb} = (U_{inc}-U_o)/U_{inc}$, where U_{inc} is the transmitted intensity measured through homogeneous intralipid solution and U_o is the transmitted intensity in the presence of the objects. It can be seen that using early photons allows the two objects to be distinguished from each other at zero degrees of rotation. Sharp edges are not observed, but it has been previously shown [11] that using early photons significantly improves the resolving power of this type of scan compared with slightly later or even CW photons.

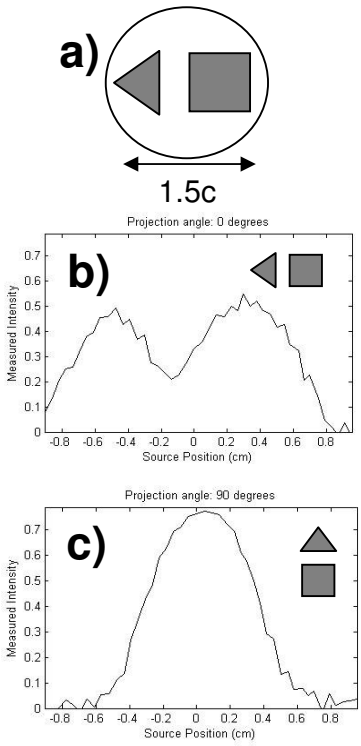

Fig. 4. (a) Phantom employed (b),(c) Line scans obtained using a linear scan of 45 sources, each corresponding to profiles similar to the ones used in Fig.3.

Figure 5 depicts a sinogram of the total data collected, in which the source position is plotted on the y-axis versus rotation angle on the x-axis. The rotation of the two absorbing heterogeneities can be clearly tracked throughout the course of the rotation. There are then several approaches to the reconstruction of the image from this measured data. One would be to assume straight line propagation of the photons as is assumed in x-ray computed tomography. This is not exactly the true photon propagation path for early optical photons, but it is a reasonable approximation and has resulted in reasonable images[11].

Reconstructions have also been achieved using singular value decomposition as shown in Fig. 6. Appropriate regularization needs to be employed for optimal results and the selection of an appropriate forward problem can further improve on reconstruction performance. Other inversion schemes could be potentially applied to further improve on image performance and more effectively handle noise. This approach can be similarly extended to fluorescence measurements. Reference data could be then collected at the excitation wavelength in the form of intrinsic measurements through a homogenous medium as also performed in this study

here or through the phantom as suggested previously using the normalized Born approach [12].

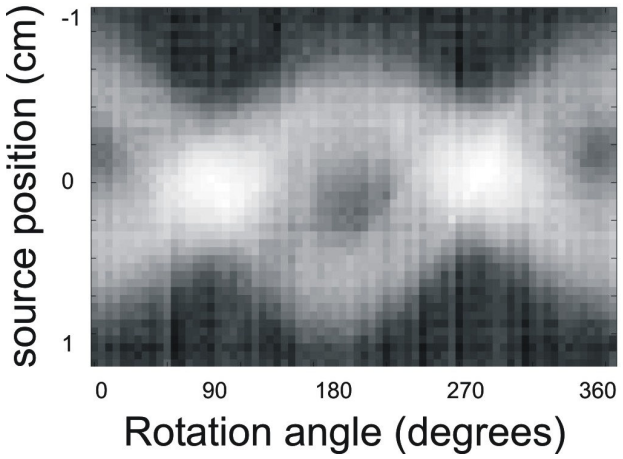

Fig. 5. Sinogram of line scans for all rotation angles

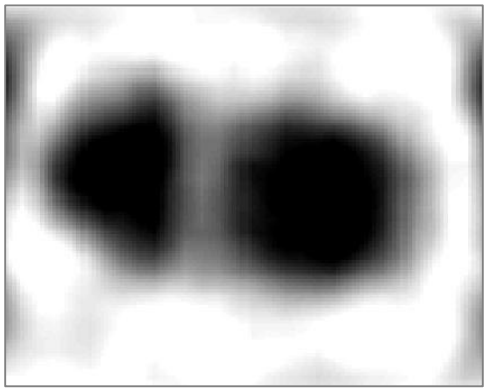

Fig. 6. Reconstructed image showing the ability to obtain shape features is shown. The result is similar to one previously obtained using the Radon transform [11].

IV. Discussion

We presented data collection and analysis steps for early photon tomography. The ability to produce complete angle projection data and employ early photons has moved optical tomography practices to approaches more common to X-ray CT tomography. The ability to produce meaningful sinograms and reconstruct edges and shapes is shown feasible and could lead to practical improvements for optical tomography. While the resolution expected between high-energy photon and near-infrared photons remains significantly different in-favor of the high energy photons due to reduced scattering experienced, the use of early near-infrared photons can be nevertheless used to improve image quality in optical tomography. This is important due to its relevance in resolving a highly advancing availability of fluorescence probes available to target and report on a broad range of molecular targets and functions.

The improvements in image quality are nevertheless done at the expense of reducing signal to noise ratio since significant portion of the signal available is not utilized. Therefore the employment of appropriate normalization schemes, signal pre-processing and inversions methods that are robust to noise become even more important than in other forms of optical tomography and are crucial in capitalizing on the maximum utility of the technique.

Acknowledgments

The authors acknowledge support from NIH grant ROI EB000750-1.

References

[1] V. Ntziachristos, C. Tung, C. Bremer, and R. Weissleder, "Fluorescence-mediated tomography resolves protease activity in vivo," *Nature Medicine*, vol. 8, pp. 757-760, 2002.

[2] V. Ntziachristos, E. Schellenberger, J. Ripoll, D. Yessayan, E. Graves, J. Bogdanov A, L. Josephson, and R. Weissleder, "Visualization of anti-tumor treatment by means of fluorescence molecular tomography using an annexin V - Cy5.5 conjugate," *Proc. Natl. Acad. Sci. U.S.A.*, vol. 101, pp. 12294-12299, 2004.

[3] B. Chance, "Optical Method," *Annual Review of Biophysics and Biophysical Chemistry*, vol. 20, pp. 1-28, 1991.

[4] R. G. Blasberg, "In vivo molecular-genetic imaging: multi-modality nuclear and optical combinations," *Nuclear Medicine and Biology*, vol. 30, pp. 879-888, 2003.

[5] D. Piwnica-Worms, D. P. Schuster, and J. R. Garbow, "Molecular imaging of host-pathogen interactions in intact small animals," *Cellular Microbiology*, vol. 6, pp. 319-331, 2004.

[6] R. Weissleder and V. Ntziachristos, "Shedding light onto live molecular targets," *Nat Med*, vol. 9, pp. 123-8, 2003.

[7] A. B. Milstein, S. Oh, K. J. Webb, C. A. Bouman, Q. Zhang, D. A. Boas, and R. P. Millane, "Fluorescence optical diffusion tomography," *Applied Optics.*, vol. 42, pp. 3081-94, 2003.

[8] M. J. Eppstein, D. J. Hawrysz, A. Godavarty, and E. M. Sevick-Muraca, "Three-dimensional, Bayesian image reconstruction from sparse and noisy data sets: near-infrared fluorescence tomography," *Proceedings of the National Academy of Sciences of the United States of America.*, vol. 99, pp. 9619-24, 2002.

[9] R. R. Alfano, S. G. Demos, P. Galland, S. K. Gayen, Y. Guo, P. P. Ho, X. Liang, F. Liu, L. Wang, Q. Z. Wang, and W. B. Wang, "Time-resolved and nonlinear optical imaging for medical applications," *Ann N Y Acad Sci*, vol. 838, pp. 14-28, 1998.

[10] E. Graves, J. Ripoll, R. Weissleder, and V. Ntziachristos, "A Sub-Millimeter Resolution Fluorescence Molecular Imaging System for Small Animal Imaging," *Medical Physics*, vol. 30, pp. 901-911, 2003.

[11] G. Turner, G. Zacharakis, A. Soubret, J. Ripoll, and V. Ntziachristos, "Complete angle projection diffuse optical tomography using early photons," *Optics Letters*, vol. in press, 2005.

[12] V. Ntziachristos and R. Weissleder, "Experimental three-dimensional fluorescence reconstruction of diffuse media using a normalized Born approximation," *Optics Letters*, vol. 26, pp. 893-895, 2001.